Graphene – A Promising Material for Organic Photovoltaic Cells

*Xiangjian Wan, Guankui Long, Lu Huang, and Yongsheng Chen**

As a promising two-dimensional nanomaterial with outstanding electronic, optical, thermal, and mechanical properties, graphene has been proposed for many applications. In this Progress Report we summarize and discuss comprehensively the advances made so far for applications of graphene in organic photovoltaic (OPV) cells, including that for transparent electrodes, active layers and interfaces layer in OPV. It is concluded that graphene may very likely play a major role in new developments/improvements in OPVs. The future studies for this area are proposed to focus on the following: i) improving the conductivity without comprising the transparency as a transparent electrode material; ii) controlling the sheet sizes, band structure and surface morphology for use as a electron acceptor material, and iii) controlling and improving the functionalization and compatibility with other materials as interface layer material.

1. Introduction

Organic photovoltaic (OPV) cells based on conjugated polymers have been of great interest due to the prospect of low-cost, solution-based processing, and fabrication on flexible substrates, which offer a significant advantage over silicon technology.[1,2] As a result of the recent and significant progress of components in the active layer, the device structure, and fabricating techniques, the performance of OPV cells has recently increased dramatically and power conversion efficiency (PCE) values of over 7% have been achieved by using low bandgap polymers in the bulk heterojunction (BHJ) structure solar cells.[3–8] Recently, a PCE of over 9% has been reported.[9] However, further improvement of the PCE and lowering cost are still mandatory requirements for the practical application of OPV cells. In general, two strategies are employed to improve the PCE. One is the design and synthesis of new materials, including donor, acceptor, and interface layer materials with superior properties. Another is to improve the device fabrication process, including understanding the device physics, structures and fabricating skills. BHJ structures based on intimate blends of electron donor and electron acceptor materials has become one of the most promising approaches for highly efficient OPV cells, since it not only maximizes the donor/acceptor interface for efficient exciton dissociation but also forms a nanoscale interpenetrating network for charge transport to the electrodes.[10] With the BHJ architecture design, although understanding of the device physics and optimizing the fabrication process are important, it seems nowadays that the key determining factor to improve PCEs is the material, including both the active layer and electrode materials. On the other hand, in order to reduce the cost for practical application, materials and fabricating process cost should also be as low as possible. As the landmark transparent electrode material, several serious issues for indium tin oxide (ITO) have been raised recently, which mainly include (i) limited source of indium on the earth; (ii) costly preparative methods such as sputtering, evaporation, pulsed laser deposition and electroplating; (iii) instability of ITO toward acid or base conditions; (iv) poor transparency in near infrared region and (v) intrinsic brittleness property for flexible devices. Therefore, it is important to find substitutive materials for ITO. Overall, in the view of the different roles of materials used in OPVs, three types of optimized materials are required in order to improve the performance and allow final practical application. These include: i) excellent active layer materials; ii) proper interface (modifying) materials; and iii) low-cost transparent electrode materials. In general, many problems in OPVs are due to the corresponding materials used, which eventually need to be solved in most cases by new material development.

Graphene, a single sheet composed of sp^2-hybridized carbon, has drawn great attention owing to its outstanding electronic, optical, thermal and mechanical properties.[11–16] Due to its unique and superior optical and electronic properties,[14] much attention is focused on its application in the field of OPV applications. Transparent electrode is one of the most comprehensive researches for graphene, which has demonstrated some great potential advantages over traditional transparent electrodes.[17,18,19] On the other hand, the unique structure and excellent electronic properties of graphene, particularly its high mobility,[20] and the handy availability of functionalized graphene, together with its chemical stability, render it a competitive alternative as the electron-accepting material in OPV applications.[21–23] While there are quite some reviews about

Dr. X. Wan, G. Long, L. Huang, Prof. Y. Chen
Key Laboratory of Functional Polymer Materials
and Centre of Nanoscale Science and Technology
Institute of Polymer Chemistry
College of Chemistry
Nankai University
300071, Tianjin, China
E-mail: yschen99@nankai.edu.cn

DOI: 10.1002/adma.201102735

graphene in many aspects,[13,15,24]including its application in energy field,[25–27] a review dedicated to its applications in OPVs is missing. In this view, we will have a comprehensive review for the progress made so far for its applications for OPVs. These include its applications for all the three major component parts in OPVs: as the material used in transparent electrode, active layer and interface layer. The application of graphene in other types of solar cells such as dye sensitized solar cell[28] or Schottky junction solar cell[29] will not be included.

Prof. Yongsheng Chen graduated from the University of Victoria with a Ph.D. degree in chemistry in 1997 and then joined the University of Kentucky and the UCLA for his postdoc studies from 1997 to 1999. Since 2003 he now holds a Chair Professor at Nankai University. His main research interests include: i) carbon-based nanomaterials, including carbon nanotubes and graphene, ii) organic and polymeric functional materials, and iii) energy devices including OPVs and supercapacitors.

2. Graphene as the Transparent Electrode Material

As the essential part of optoelectronic devices, the ideal transparent electrodes should have high transparency (>80%), low sheet resistance (<100 Ω/sq.) and proper work function (4.5-5.2 eV). In addition, the cost including preparation of the transparent electrode and fabrication of the device should also been equally considered. Currently, ITO plays a dominant role and is the market standard for most of transparent electrode applications. In OPV cells, ITO have been used as the hole collecting electrode with transparencies of >90% at the wavelength of 550 nm, sheet resistances of 10-30 Ω/sq and a favorable work function. As mentioned above, the use of ITO as transparent electrode could be limited due to its intrinsic drawbacks, and thus it is highly needed to develop new transparent conducting materials. Carbon nanotubes (CNTs) have been studied as an alternative for ITO. The PCE of OPV cells using CNTs as the transparent electrode has reached 2.5%,[30] which is comparable to the reference device with ITO as the electrode under similar conditions. However, the high surface roughness of the CNT film and highly energy consuming in CNTs preparation (CVD or arc discharge) may limit its further application. In contrast to CNTs, graphene is a one-atom thick, two-dimensional material with excellent electron transport properties and is believed to be one of the most promising materials for transparent electrode applications. Several excellent reviews have discussed the updated progress and broad applications of the transparent electrodes based on graphene.[18,19,31] Herein, we put our attention on the graphene based transparent electrodes used for OPV cells.

The preparation of transparent conductive graphene films over large areas and at low cost are the key issues for their potential applications in OPV cells. Among the conventional methods to obtain graphene thin films such as micromechanical exfoliation,[20] epitaxial growth,[32] chemical vapor deposition (CVD)[33] and reduction of graphene oxide (GO),[34–36] the last method using solution process with GO has been primarily used to prepare graphene films as transparent electrodes because of the advantages of high throughput preparation, low cost, and the simplicity of the fabrication technique.

Chen et al. have demonstrated solution-processed polymer OPVs using the neat reduced graphene oxide (rGO) film as the transparent anode, with poly-(3-hexylthiophene) (P3HT) as the electron donor and phenyl-C_{61}-butyric acid methyl ester (PCBM) as the acceptor (**Figure 1**a).[37] After spin-coating deposition, the insulating GO films are reduced through exposure to hydrazine vapor and then annealed under inert conditions to render the material electrically conductive. The electrical conductivity of as-prepared graphene film is closely related to the annealing temperature. At a given film thickness of ~25 nm, concomitant increase of film conductivity was observed with an increase in the annealing temperatures from 300 to 700°C (Figure 1b). The graphene films could have a sheet resistance of 17.9 KΩ/sq (transmittances of 69% at 550 nm) and a conductivity of 22.3 S/cm. The device under illumination of simulated solar light (AM 1.5G) shows a short-circuit photocurrent density (J_{sc}) of 1.18 mA/cm^2, an open-circuit voltage (V_{oc}) of 0.46 V, a filling factor (FF) of 0.25, and PCE of 0.13%. The low PCE is likely due to the high sheet resistance of graphene films and the hydrophobic graphene film surface, which makes it rather hard to get a uniform PEDOT:PSS layer.

Similarly, Wu et al. used rGO as transparent conductive anodes for organic bilayer small molecules OPV cells.[38] The transparent electrodes based on graphene were obtained by vacuum annealing of GO or by a combination of a hydrazine treatment and argon annealing at 400 °C. For the film thicknesses of <20 nm, the optical transmittance is generally >80%, while the sheet resistance varies from 5 kΩ/sq to 1 MΩ/sq. The thickness of graphene films used to fabricate OPV cells is between 4 and 7 nm, and the corresponding values of the transmittance and sheet resistance are 95%-85%, and 100 to 500 kΩ/sq, respectively. Devices with structure of anode/CuPc/C_{60}/BCP/Ag were fabricated. The J_{sc}, V_{oc}, FF, and PCE for the cell on graphene are 2.1 mA/cm^2, 0.48 V, 0.34, and 0.4%, respectively; and that for the cell on ITO as a comparison are 2.8 mA/cm^2, 0.47 V, 0.54, and 0.84%, respectively. The poor performance is mainly caused by the high sheet resistance of the graphene thin films, and improved graphene film treatments should be required to reduce the sheet resistance without compromising transmittance.

Yin et al. fabricated flexible OPV devices by using a transferred rGO film as the transparent electrode (Figure 1c-f).[39] The authors found that lowering the rGO sheet resistance via increasing the rGO film thickness notably enhances the J_{sc} of devices and thus the overall PCE, even if the transmittance of rGO film decreases. The highest PCE obtained is 0.78% by employing a flexible rGO/polyethylene terephthalate (PET)-based transparent electrode with a transparency of 55% and resistance of 1.6 kΩ/sq. These devices show an excellent

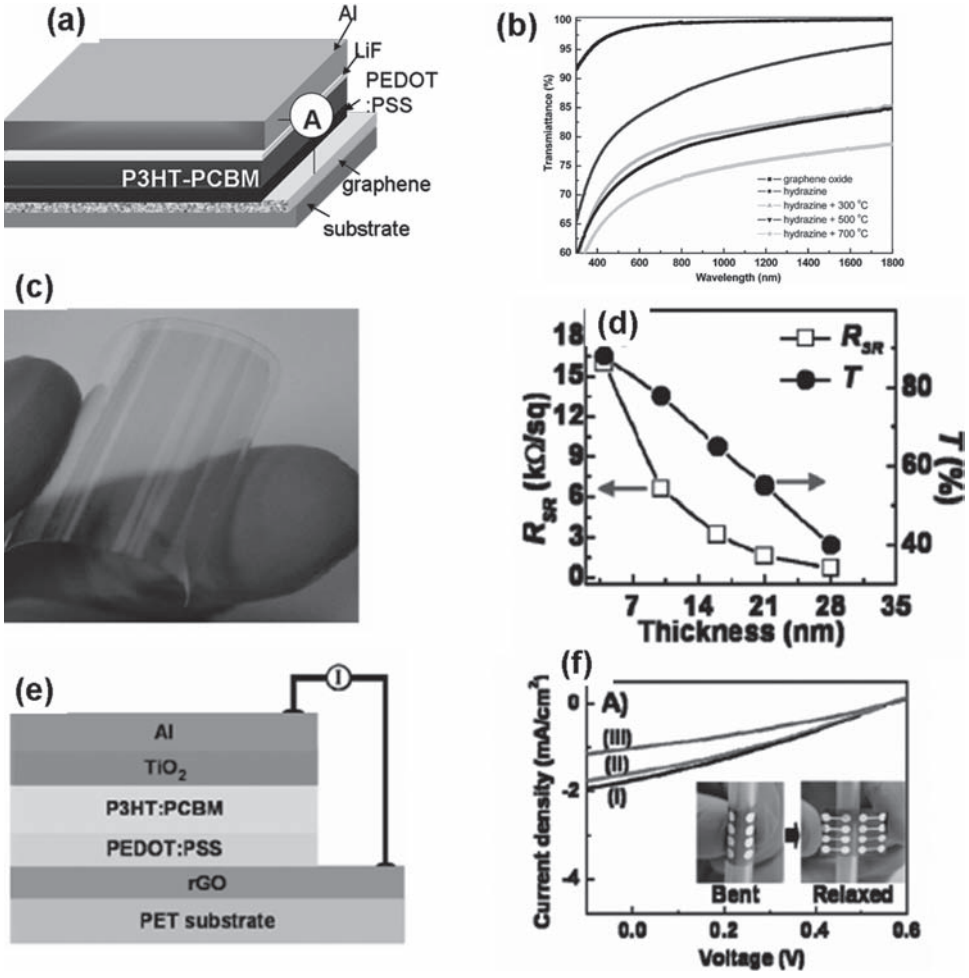

Figure 1. (a) Device structure and energy diagram of the fabricated device with structure quartz/graphene/PEDOT:PSS/P3HT:PCBM/LiF/Al. (b)Optical transmittance spectra of GO film (~40 nm) and graphene films (~25 nm) with different reduced methods. (c) Photograph of rGO/PET. (d) Sheet resistance (R_{SR}) and transmittance (T) of rGO film as a function of its thickness. (e) Schematic representation of the device structure. (f) Current density-Voltage (J-V) curves of the device 1 after applying (i) 400, (ii) 800, and (iii) 1200 cycles of bending. (a-b) Reproduced with permission.[37] Copyright 2010, Elsevier. (c-f) Reproduced with permission.[39] Copyright 2010, ACS.

stability after applying the bending induced tension stress, and their performance can be well maintained even after bending a thousand times.

Eda et al. reported the preparation of transparent and conductive graphene films by vacuum filtration of GO solution to form the GO film, followed by a combination of hydrazine vapor and low temperature annealing (200 °C) in nitrogen or vacuum (**Figure 2**a,b).[40,41] The conductivity of the thin films can be varied over six orders of magnitude by varying the filtration volume of the GO aqueous solutions while maintaining the transmittance between 60%-95%. In addition, the conductivity of rGO film could be enhanced through Cl doping using $SOCl_2$. After doping, the sheet resistance of the rGO thin film could be reduced by a factor of nearly 5, while for the thicker films the effect of doping was moderate (Figure 2c). Using these graphene films as the transparent electrode, OPV cells with a blend of P3HT and PCBM as the active layer and aluminum as the top electrode were fabricated. The PCE was approximately 0.1%, which is obviously limited by the large resistance at the order of 10^5 Ω/sq for the rGO electrodes.

Geng et al. reported the preparation of transparent conductive graphene films by a two-step reduction method that consisted of the controlled chemical reduction of GO in an aqueous suspension and the thermal annealing of the resultant films at temperatures of 200, 400, and 800 °C (Figure 2e).[42] The authors indicated that the two step reduction approach not only effectively restored the sp^2 carbon networks of the chemically converted graphene (CCG) sheets but also reduced the interlayer distance in the CCG films. These features led to enhanced charge carrier transport in the individual CCG sheets and increased charge carrier transport across the CCG sheets. Using the CCG-A800 films (80% transparency at 550 nm, sheet resistance 10^3 Ω/sq) as transparent electrodes, OPV BHJ devices (Figure 2f) with P3HT and PCBM as active layer showed a PCE of 1.01 ± 0.05%, which is higher than that of the OPV devices using rGO as the transparent electrode.

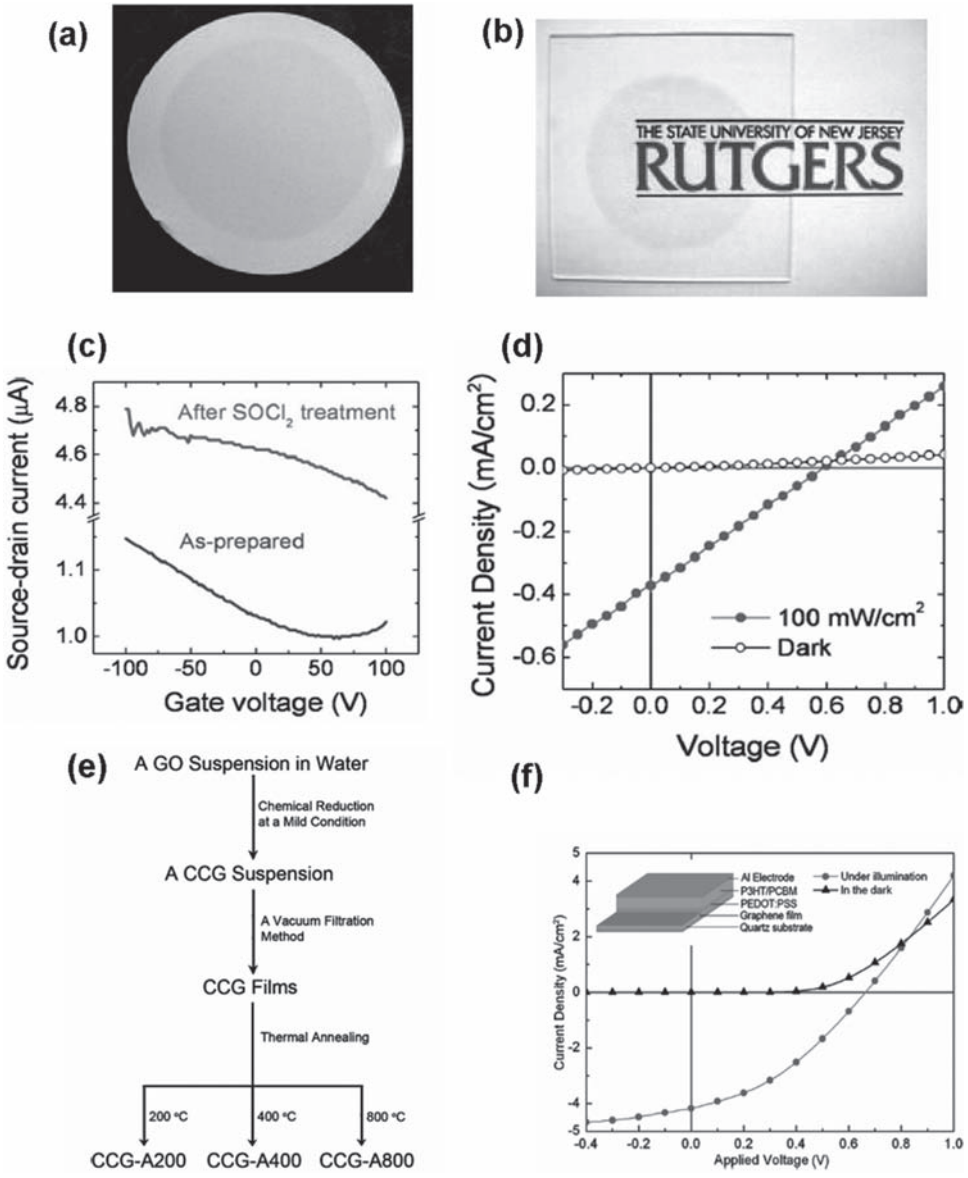

Figure 2. (a) Photographs of GO thin films on filtration membrane (a), glass (b). (c) Transfer characteristics of a reduced GO thin film before and after dipping in $SOCl_2$ for 1 h. The film was prepared at a filtration volume of 30 mL with 0.33 mg/L GO suspension and transferred onto a Si substrate with 300 nm thermally grown oxide. Au was used as source and drain electrodes and the channel length was 21 μm. The gate voltage was swept from positive to negative with 1 V step. (d) Solar cell characteristics of an OPV with a reduced GO thin film as the transparent electrode. A Newport AM1.5 solar simulator was used to evaluate the photovoltaic characteristics. The film used for the fabrication of OPV had thickness of ~14 nm, sheet resistance of ~40 kΩ/sq, and transmittance of 64%. (e) Schematic illustration of the preparation of transparent conductive graphene films. (f) J-V curves for a P3HT:PCBM solar cell device made using the CCG-A800 film as a transparent electrode. The inset shows the configuration of the solar cell device. (a-b) Reproduced with permission.[40] Copyright 2008, Nature publishing group. (c-d) Reproduced with permission.[41] Copyright 2008, AIP. (e-f) Reproduced with permission.[42] Copyright 2010, ACS.

Probably, the most important reason for the current limited performance of OPV cells employing graphene as the transparent electrode material is the high sheet resistance of graphene films used therein. A strategy to improve the conductivity is to incorporate a conductive material with graphene. Tung et al. reported a hybrid nanocomposite comprised of graphene and carbon nanotubes (G-CNT) (**Figure 3**a).[43] By introducing CNTs, the conductivity of the hybrid material was enhanced, while sacrificing little in transparency. G-CNT film by spin-coating with sheet resistance of 240 Ω/sq and 86% transmittance was obtained. In addition, the G-CNT hybrid film exhibited better mechanical stabilities than ITO (Figure 3b). P3HT:PCBM BHJ device (Figure 3c) using G-CNT hybrid material as the transparent electrode exhibited a PCE of 0.85%. The J_{sc}, V_{oc}, and FF were 3.47 mA/cm^2, 0.583 V, and 0.42, respectively. The low J_{sc} and FF are likely due to the poor contact at the interface between the G-CNT and the polymer blend.

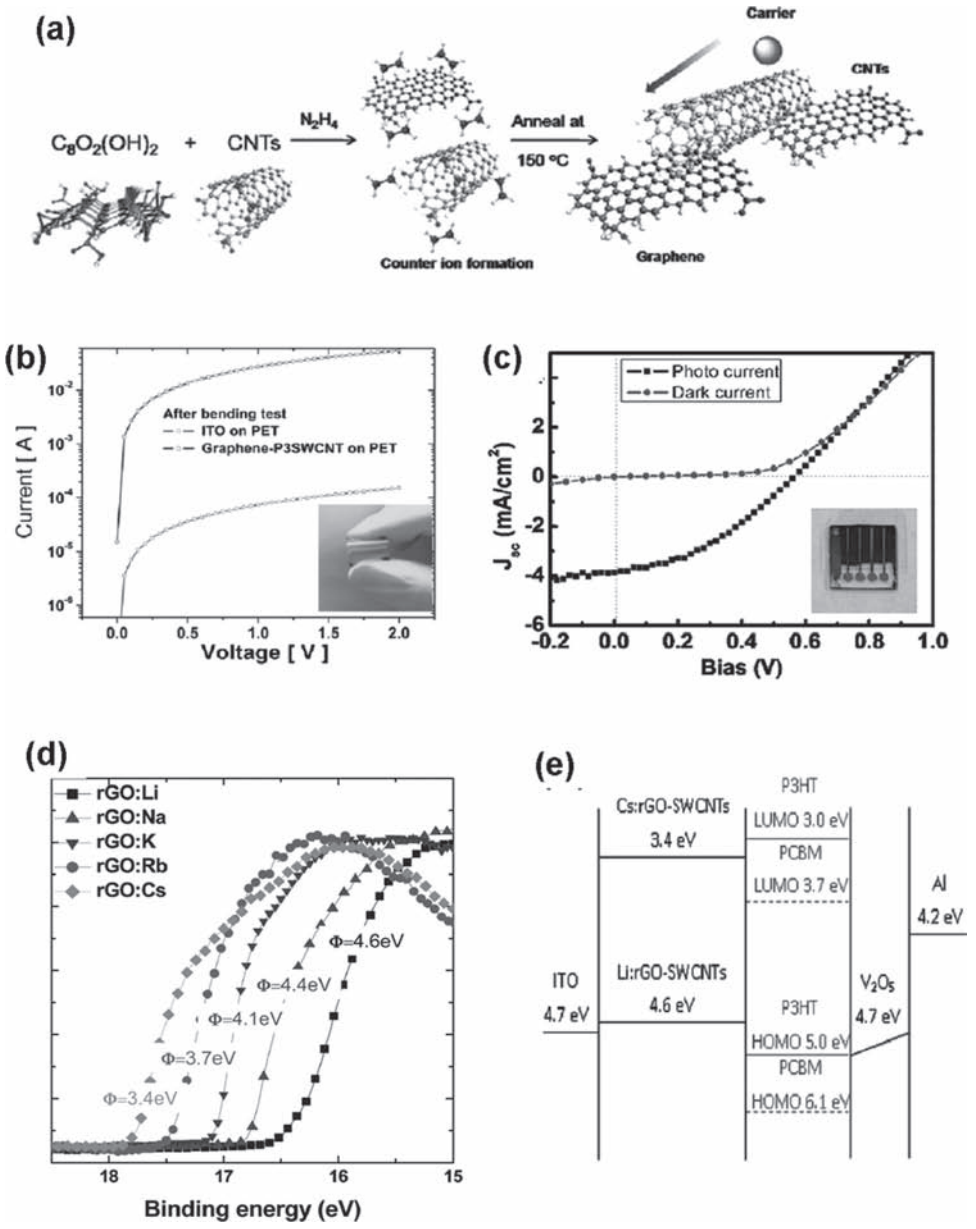

Figure 3. (a) Scheme of preparation for the graphene carbon nanotube hybrid; (b) Electrical measurements of G-CNT and ITO films after bending at 60 ° 10 times. The ITO resistance increases 3 orders of magnitude, while the resistance of the G-CNT hybrid electrode remains; (c) J-V curves of G-CNT based organic solar cell device consists of G-CNT (5 nm)/PEDOT (25 nm)/P3HT:PCBM (230 nm)/Ca:Al (80 nm). (e) UPS spectra of the rGO doped with various alkali carbonates. The pronounced peaks for the alkali metals indicate the successful doping of the alkali carbonates. The values of Φ_w of the rGO-SWCNT films were determined from the UPS secondary electron cutoff. (f) Energy level diagrams of inverted solar cells featuring alkali carbonate-doped carbon-based cathodes. (a-c) Reproduced with permission.[43] Copyright 2009, ACS. (d-e) Reproduced with permission.[44] Copyright 2011, ACS.

In addition to requiring high conductivity and transparency, the transparent electrode used in OPV cells should have proper work function to minimize the energy barriers for charge injection. Most recently, Huang et al. reported a strategy for tuning the work function (Φ_w) of solution-processed rGO-SWCNT composite films through doping with alkali carbonates (Figure 3d-e).[44] The pristine rGO-SWCNT electrode exhibited a Φ_w value of 5.1 eV. After doping, the values of Φ_w decreased from 4.6 eV to 3.4 eV. The formation of interfacial dipoles was presumed to be the reason for decreasing the work function of the rGO-SWCNTs composites. Inverted P3HT/PCBM solar cells employing $CsCO_3$ doped rGO-SWCNTs as the transparent electrode (transparency 65.8% at 550 nm and sheet resistance 331 Ω/sq) was fabricated and gave PCE of 1.27%, which is comparable with that of the normal structure device.

Su reported composites of reduced graphene sheets (ReG) with large aromatic molecules pyrene-1-sulfonic acid sodium salt (PyS) and diasodium salt of 3,4,9,10-perylenetetracarboxylic

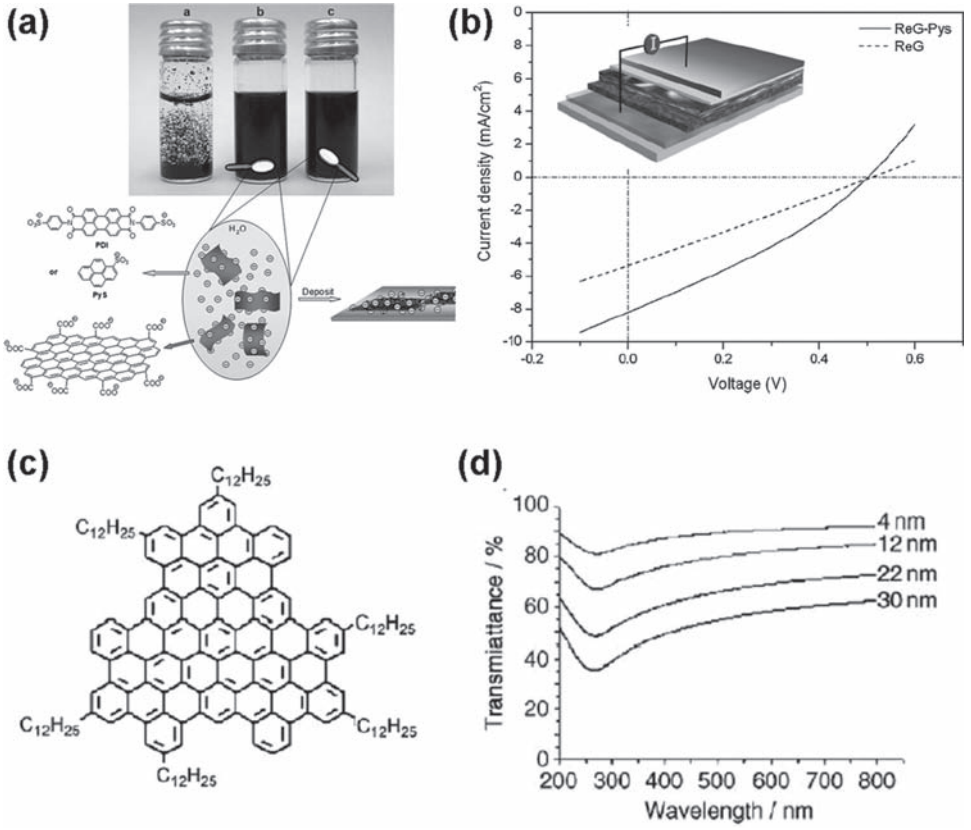

Figure 4. (a) Schematic illustration and images of aqueous dispersions of graphene sheets (0.25 mg/mL) and composites on the surface: a) ReG aqueous dispersion, black precipitate after reduction; b) ReG-PDI aqueous dispersion, without precipitate after centrifugation (5000 rps/30 min); c) ReG-PyS aqueous dispersion, without precipitate after centrifugation (5000 rps/30 min). (b) J–V curves of P3HT/PCBM heterojunction solar cells with 10 nm thick thermally reduced ReG and ReG-PyS films as the transparent electrodes, respectively. Inset is the schematic illustration of the solar cell; the five layers from top to bottom are Al, ZnO, a blend of P3HT and PCBM, PEDOT:PSS, graphene, and quartz, respectively. (c) Molecular structure of TGF, the hexadodecyl-substituted superphenalene C96-C12. (d) Transmission spectrum of the TGFs with different thicknesses. (a-b) Reproduced with permission.[45] Copyright 2009, Wiley-VCH. (c-d) Reproduced with permission.[46] Copyright 2008, Wiley-VCH.

diimide bisbenzenesulfonic acid (PDI) (**Figure 4**a,b).[45] The conductivities of both ReG-PDI and ReG-PyS were dramatically increased to >1100 S/cm when annealed at 1000 °C, about twice as high as that of pristine ReG (517 S/cm), indicating an improved π-conjugation upon "doping" of graphene sheets with these molecules. An improvement of the overall PCE from 0.78 to 1.12% was achieved using ReG-PyS as the anode electrode in BHJ solar cells instead of pristine ReG. These results indicate that the combination of large aromatic molecules and graphene sheets could generate desirable electrode materials that qualify for photovoltaic devices.

Wang et al. reported a bottom-up chemical approach towards the synthesis of transparent graphene-constructed films (TGFs) as electrodes (Figure 4c,d).[46] The graphene films prepared by using the bottom-up approach with thicknesses of 4, 12, and 22 nm exhibited transparencies of 90, 80, and 66% at wavelength of 500 nm, respectively. With the above graphene films as transparent electrodes, a BHJ structure OPV cell using a blend of P3HT and PCBM as the active layer was fabricated. Under the monochromatic light with the wavelength of 510 nm, the PCE of the TGF based solar cell was 1.53%, which was almost the same as that of the ITO-based cell (1.5%). However, under the illumination of the simulated solar light, the PCE was 0.29%, which was lower than that of the ITO-based cell (1.17%).

Chemical vapor deposition (CVD) is an important and successful method to obtain high-quality graphene films.[47–49] For example, graphene films with sheet resistance of 280 Ω/sq (80% transparency) and 770 Ω/sq (90% transparency) prepared on Ni coated SiO_2/Si wafer by CVD have been reported.[33] Large-area graphene films produced by CVD process were reported by Wang et al. and used as transparent electrode in OPVs.[50] For 6-30 nm thick graphene films, the average sheet resistance varies from 1350 to 210 Ω/sq with an optical transparency from 91% to 72% in the visible light wavelength range. As shown in **Figure 5**, a BHJ structure solar cell using the graphene anode was fabricated. The J_{sc}, V_{oc}, FF, and PCE are 2.39 mA/cm^2, 0.32 V, 0.27, and 0.21%, respectively. The poor performance was caused by the hydrophobic property of graphene, which prevent to have the uniform coating of PEDOT:PSS. After a UV treatment of graphene film for 10 min to improve the surface wettability, the device PCE was increased to 0.74%. In order

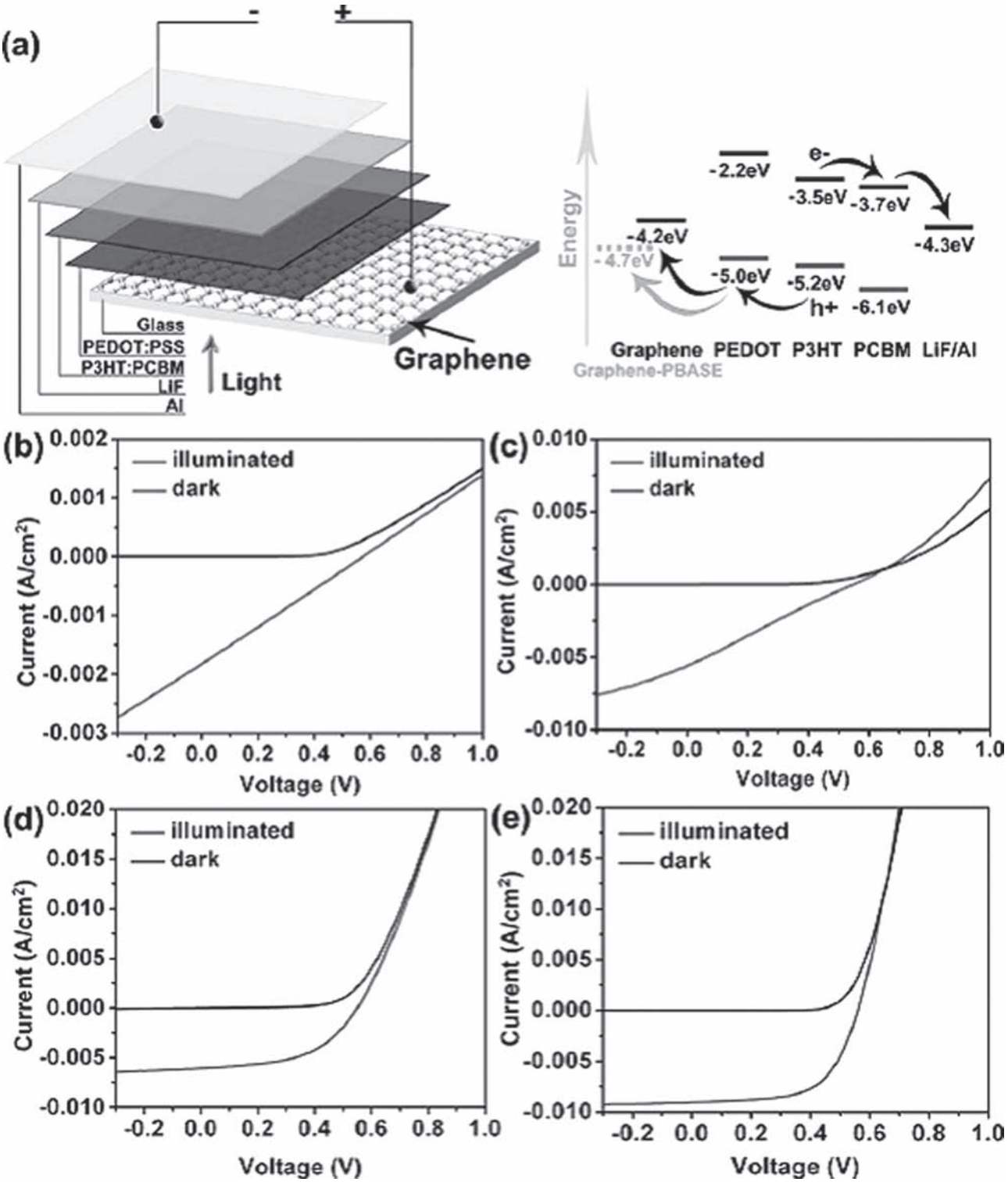

Figure 5. (a) Energy diagram of the fabricated device with structure graphene/PEDOT:PSS/P3HT:PCBM/LiF/Al.(b)-(e) Current voltage characteristics of the photovoltaic devices based on graphene films in dark and under illumination, where (b) is from pristine graphene film, (c) graphene film treated by UV light, (d) graphene film modified by PBASE. (e) ITO anode for comparison. Reproduced with permission.[50] Copyright 2009, AIP.

to avoid the disruption of the aromatic structures caused by covalent bonding with oxygen groups after the UV treatment, the graphene anode was modified by self-assembled pyrene buanoic acid succidymidyl ester (PBASE). A well improved performance (V_{oc} = 0.55 V, J_{sc} = 6.05 mA/cm^2, FF = 0.51, and PCE = 1.71%) was obtained. In contrast, the device made with

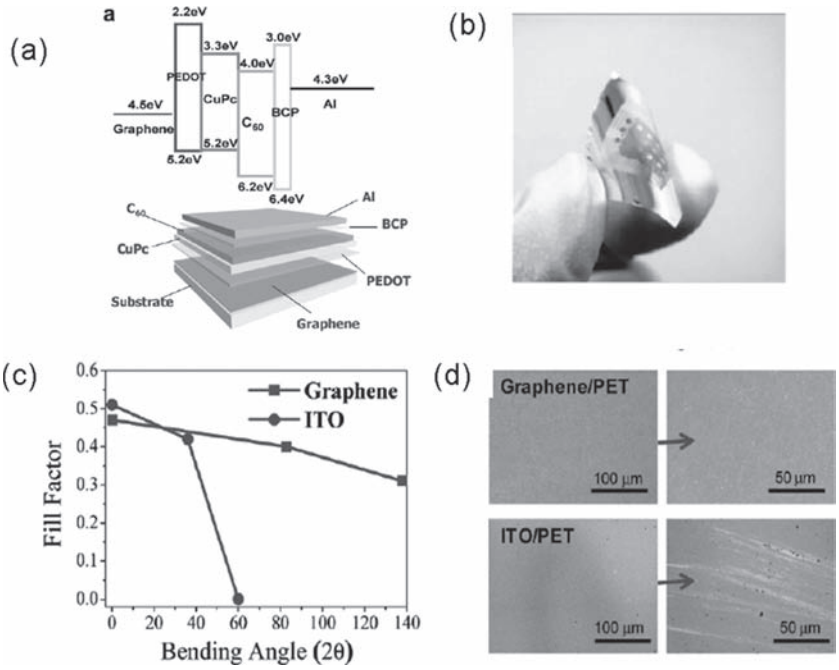

Figure 6. (a) Schematic representation of the energy level alignment (top) and construction of the heterojunction organic solar cell fabricated with graphene as anodic electrode: CVD graphene/PEDOT/CuPc/C_{60}/BCP/Al. (b) Photograph illustrating high flexibility of CVD graphene transferred on a PET flexible substrate. (c) Fill factor dependence of the bending angle for CVD graphene and ITO devices. (d) SEM images showing the surface structure of CVD graphene (top) and ITO (bottom) photovoltaic cells after being subjected to the bending angles. (a-d) Reproduced with permission.[51] Copyright 2010, ACS.

ITO anode showed V_{oc}, J_{sc}, FF, and PCE of 0.56 V, 9.03 mA/cm^2, 0.61, and 3.10%, respectively.

Arco et al. reported a transparent graphene film by CVD with sheet resistance 230 Ω/sq and transparency 72% at a wavelength 550 nm,[51] its sheet resistance is much lower than the stacked graphene flakes at similar transparency (**Figure 6**). Using CVD graphene and ITO electrodes as the anodes, OPV cells using these two types of anodes and with same structure of PEDOT:PSS/CuPc/C_{60}/BCP/Al on flexible PET substrates offer comparable performance, with PCE 1.18% and 1.27%, respectively. In addition, the above CVD graphene solar cells demonstrated capability to operate under bending conditions up to 138°, whereas the ITO-based devices displayed cracks and irreversible failure under bending of 60°. This work indicates the great potential of CVD graphene films for flexible photovoltaic applications.

Lee and his coworkers reported the preparation of multilayer graphene (MLG) film grown by CVD and its application as transparent electrodes in organic BHJ solar cells with the active layer using a mixture of P3HT/PCBM.[52] The 1000 °C-grown MLG films with sheet resistances of 606 Ω/sq and transmittances of 87% showed the best performance as the electrodes for OPV devices. After the cell structure optimization with an inserted TiO_X layer (**Figure 7**a,b), the PCE was enhanced up to 2.58 ± 0.45%. In addition, the work function of above MLG film grown could be tuned by using thin interfacial dipole layers.[53] The work function of pristine MLG 4.58 eV was reduced to 4.25 eV using poly[9,9-bis((6'-(N,N,N-trimethylammonium)hexyl)-2,7-fluorene)-alt-(9,9-bis(2-(2-(2-methoxyethoxy)ethoxy)ethyl)-9-fluorene)]dibromide (denoted as WPF-6-oxy-F, Figure 7d) as an interfacial layer. BHJ device with an inverted structure (Figure 7c) MLG/WPF-6-oxy-F/P3HT:PCBM/PEDOT:PSS/Al gave PCE 1.23%, which was about half of the PCE 2.23% for the cells using WPF-6-oxy-F functionalized ITO electrodes for comparison.

Loh et al. reported a direct layer-by-layer (LBL) transfer method of CVD graphene sheets that was free from the possible residual impurity in the conventional transfer process between the layers (**Figure 8**).[54] The LBL, acid-doped, four layer graphene film exhibited a sheet resistance of 80 Ω/sq and a transmittance of 90% at 550 nm, which is comparable to the ITO. For device fabrication, a thin layer MoO_3

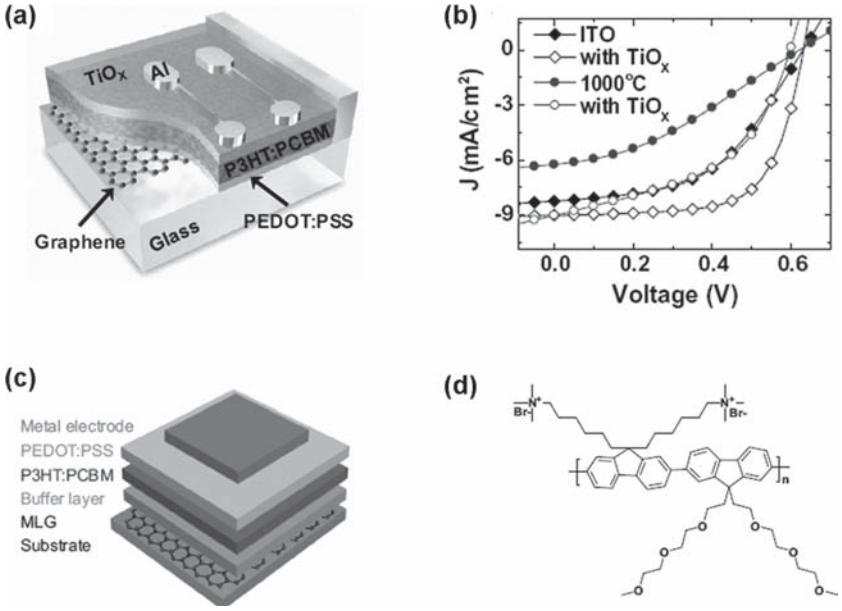

Figure 7. (a) Schematic diagram of the photovoltaic device structure with MLG electrodes and a hole-blocking TiO_X layer. (b) J-V curves of photovoltaic devices with 1000 °C-grown MLG electrodes (circles) and with ITO electrodes (diamonds). The curves without the TiO_X layer (filled symbols) are compared to the ones with the TiO_X layer (open symbols). (c) Schematics of an inverted-structure OPV with the work-function-engineered MLG electrode. (d) Molecular structure of WPF-6-oxy-F. (a-b) Reproduced with permission.[52] Copyright 2010, Elsevier. (c-d) Reproduced with permission.[53] Copyright 2010, ACS.

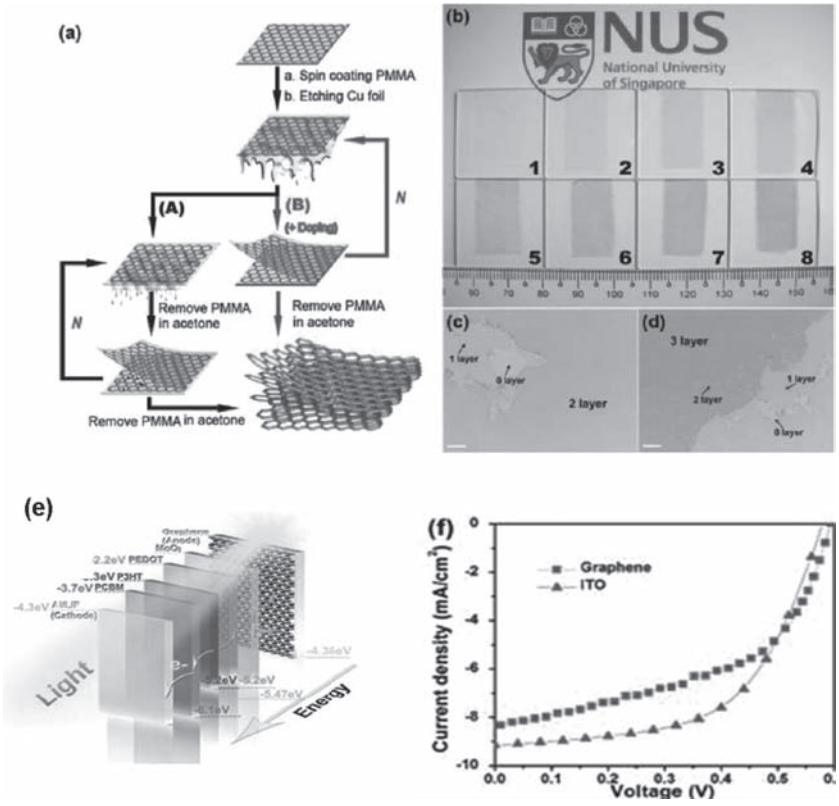

Figure 8. (a) Schematic drawing of multilayer graphene films made by normal wet transfer (A) and direct coupling LBL assembly (B) (N = 0,1,2,3…). (b) Optical image of multilayer graphene films (from 1 to 8 layers) on a quartz substrate. (c,d) Typical optical microscope images of 2- and 3-layer graphene films on SiO_2/Si substrates. (e) Schematic diagram of photovoltaic device structure. (f) anode/PEDOT:PSS/P3HT:PCBM/LiF/Al (anode is ITO or MoO_3-coated graphene). (a-f) Reproduced with permission.[54] Copyright 2011, Wiley-VCH.

was evaporated on the graphene to improve its hydrophility for spin coating of PEDOT:PSS. In addition, presence of MoO_3 could shift the work function of graphene film from 4.36 to 5.47 eV. 4-layer acid-doped graphene solar cells with the structure of graphene/MoO_3/PEDOT:PSS/P3HT:PCBM/LiF/Al exhibited the best performance with a PCE of 2.5%, V_{oc} of 0.59 V, J_{sc} of 8.5 mA/cm^2 and FF of 0.51. In contrast, the ITO device has a PCE of 3%, V_{oc} of 0.58 V, J_{sc} of 9.2 mA/cm^2 and FF of 0.57.

As discussed above, the hydrophobic graphene film surface makes it rather hard to get uniform PEDOT/PSS layer. Unlike for ITO, O_2 plasma treatment could disrupt the aromatic rings of graphene and reduce its conductivity seriously, especially for single or few-layer graphene electrode. Park et al. reported that $AuCl_3$ doping on CVD grown graphene films could alter the graphene surface wetting properties, thus a uniform coating of the hole transport layer (HTL) could be achieved after such treatment.[55] In addition, the doping could also improve the conductivity and shift the work function of the graphene electrode. As shown in **Table 1**, the overall performance is comparable with pristine graphene electrodes, and slightly inferior to their counterparts with ITO electrodes due to the higher sheet resistance than ITO.

A summary of best PCEs employing graphene based transparent electrodes in OPV devices are presented in **Table 2**. The results demonstrate that transparent conductive graphene films exhibit great potential as window electrodes in OPV cells. However, significant improvement is needed. Several factors need to be considered in the future studies: 1) the compromise between conductivity and transparency. High sheet resistance is one of the main factors for the still limited performance of the devices employing graphene as the transparent electrodes. Defects are the main factors for high resistance of graphene films. In order to improve the conductivity without sacrifice of the transparency, recovery of the graphene intrinsic structure as much as possible should be firstly considered. On the other hand, chemical doping or formation of hybrid materials by introducing a high conductive material has also demonstrated to be an effective approach for improving the conductivity. 2) The hydrophility of graphene films, which has to be improved to allow the formation of a smooth and uniform layer of hole-transporting material such as PEDOT:PSS. Surface modification seems to be better than the UV/ozone treatment owning to the disruption of the aromatic structure of graphene films and decreasing of the conductivity when using the latter method. On the other hand, employing and developing a hydrophobic interface layer might be another effective way to be compatible with graphene surface. Certainly, if the work function of graphene films could be tuned to match with that of the active layer, no interface layer would be needed. 3) The cost for preparation and 4) the possibility in large scale production. For commercialization, low cost and large scale production are required for the graphene based transparent electrode. In addition, roll to roll process is the primary consideration for low cost and large scale production for OPVs.

Table 1. Summary of photovoltaic performance parameters of OPVs with $AuCl_3$ doped graphene as transparent electrode. Reproduced with permission. [55] Copyright IOP Publishing.

Device [a]	V_{oc} (V)	J_{sc} (mA/cm$_2$)	FF	PCE(%)
ITO/PEDOT:PSS	0.45	6.48	0.46	1.33
Pristine graphene/PEDOT:PSS	0.48	3.46	0.45	0.75
Doped grapheme [b]/PEDOT:PSS	0.46	6.44	0.52	1.51
ITO/PEDOT:PSS [c]	0.46	6.88	0.56	1.77
Pristine graphene/PEDOT:PSS[c]	0.49	6.32	0.44	1.37
Doped graphene[b]/PEDOT:PSS[c]	0.43	9.15	0.42	1.63

[a]graphene or ITO/PEDOT:PSS (or other equivalent layer)/CuPc/C_{60}/BCP/Ag (or Mg/Ag); [b]Graphene chemically doped (p-type) with $AuCl_3$ in nitromethane (10 mM); [c]PEDOT:PSS treated with O_2 plasma prior to active layer deposition.

Table 2. Summary of graphene based electrodes and best PCEs employing them in OPV cells.

Graphene material	Sheet resistance	T (%)	Device structures [a]	PCE (%)	Ref.
rGO	17.9 kΩ/sq	69	G/PEDOT:PSS/P3HT:PCBM/LiF/Al	0.13	[37]
rGO	100-500 kΩ/sq	85-95	G/CuPc/C_{60}/BCP/Ag	0.4	[38]
rGO	1.6 kΩ/sq	55	GPEDOT:PSS/P3HT:PCBM/TiO_2/Al	0.78	[39]
rGO	40 kΩ/sq	64	G/PEDOT:PSS/P3HT:PCBM/Al	0.1	[40,41]
rGO	1 kΩ/sq	80	GPEDOT:PSS/P3HT:PCBM/Al	1.01	[42]
rGO-CNT	240 Ω/sq	86	G/PEDOT:PSS/P3HT:PCBM/Ca:Al	0.85	[43]
rGO-SWCNTs-$CsCO_3$	331 Ω/sq	65.8	G/P3HT:PCBM/V_2O_5/Al	1.27	[44]
rGO-Pys	916 S/cm	68	G/PEDOT:PSS/P3HT:PCBM/ZnO/Al	1.12	[45]
bottom-up synthesis	18 kΩ/sq	85	G/P3HT:PCBM/Ag	0.29	[46]
CVD	210 to 1350 Ω/sq	72 to 91	G/PEDOT:PSS/P3HT:PCBM/LiF/Al	1.71	[50]
CVD	230 Ω/sq	72	G/PEDOT:PSS/CuPc/C_{60}/BCP/Al	1.27	[51]
CVD	606 Ω/sq	87	GPEDOT:PSS/P3HT:PCBM/TiO_X/Al	2.58	[52]
CVD	850 to 520 Ω/sq	90 to 85	G/WPF-6-oxy-F/P3HT:PCBM/PEDOT:PSS/Al	1.23	[53]
CVD	80 Ω/sq	90	G/MoO_3/PEDOT:PSS/P3HT:PCBM/LiF/Al	2.5	[54]
CVD-$AuCl_3$	500 to 300 kΩ/sq	97.1 to 91.2	G/PEDOT:PSS/CuPc/C_{60}/BCP/Ag	1.63	[55]

[a] "G" represents graphene based transparent electrode.

How to fulfill the requirement of roll to roll process is also a challenge for graphene based transparent electrode. Overall, graphene films from rGO demonstrate great advantages such as low cost, solution process and large production and would be preferred for the transparent electrode in OPV application.

3. Graphene as an Acceptor Material

In contrast to the traditional inorganic semiconductors where free electrons and holes are easily generated under solar illumination, in OPV cells, a strongly bound electron-hole pair (exciton) is generated. An energetic driving force must exist to separate this Coulombic bound electron-hole pair. In OPV devices, the separation of the photoexcited electron-hole pairs can be achieved by creating a heterojunction with the acceptor material, which has a larger electron affinity (EA) than that of the donor polymers, but still smaller than its ionization potential (IP). Owing to difference of EA and IP for the two materials, the heterojunction supplies the driving force for charge separation, which is necessary to dissociate the tightly bound electron-hole pairs into separated charges. Two types of heterojunctions have been widely used: bilayer or planar heterojunction structure[56] and an intermixed bulk heterojunction (BHJ) structure.[10] The efficiency of the planar heterojunction device is restricted by the rather limited exciton diffusion length, which is the distance over which excitons have to travel before reaching the charge transport channels. This has been called the exciton diffusion bottleneck.[57,58] The exciton diffusion bottleneck can be effectively reduced by applying the BHJ structure, where all excitons are formed hopefully within the exciton diffusion length in an interpenetrating network of the donor and acceptor materials. Currently, the most successful OPV devices are fabricated using the BHJ structure, with low band gap polymers as the donor and fullerene derivatives such as PCBM as the acceptor. In contrast to the intensive investigation for the design and synthesis of low band gap donor materials,[59,60] unfortunately, few acceptor materials other than the fullerene derivatives have been developed to address overall the OPV performance.[61] As the most widely used acceptor, C_{60} based acceptors have some limits[62,63], e.g. very weak absorption in the visible range, low LUMO energy level which is difficult to tune for high open circuit voltage in BHJ devices. Although much effort has been made on modifying fullerene and its derivatives, only slight improvements have been achieved. This has prompted studies for new acceptor materials with energy levels different from those of C_{60} derivatives.[64,65] CNTs have unique characteristics, such as high charge mobility, long π–π conjugation and large aspect ratio, however, the efficiency of photovoltaic cells based on the acceptor of CNTs is rather low so far in BHJ devices, usually below 0.5%.[66] This is because of a number of factors such as impurities in CNTs, insolubility of the CNTs in common solvents, their polydispersity in length and diameter and the nature as a mixture of metallic and semimetallic types.[67] Graphene exhibits high electron mobility than fullerene derivatives and its energy level can be tuned easily through controlling its size, layers and functionalization. Importantly, it can be easily dispersed in organic solvent after simple functionalization, thus solution process can be employed. When mixed with conjugated polymers (in general with low EA), a heterojunction is expected to be formed owing to the difference of EA. In addition, large donor/acceptor interfaces for charge generation and a continuous pathway for electron transfer will be formed owing to the large two-dimensional plane structure and one-atom thickness property of graphene. So, it is expected that graphene could be a good candidate for the acceptor material in OPV applications.

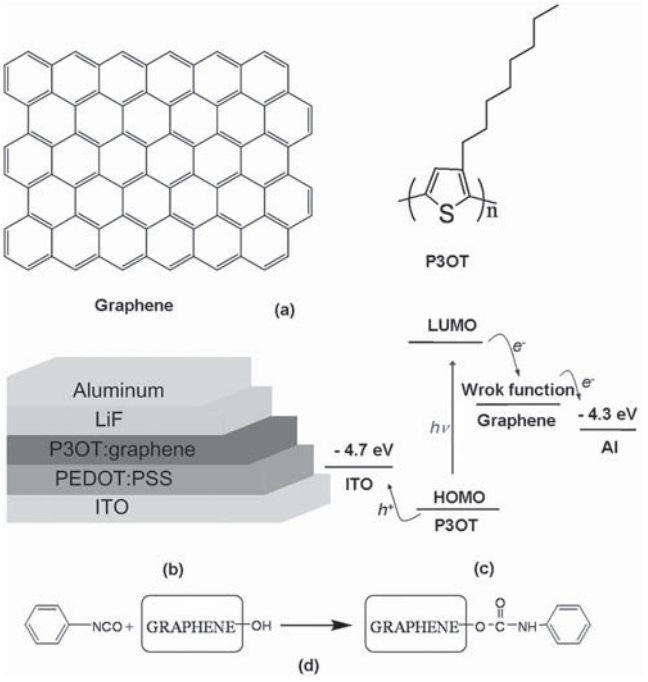

Figure 9. (a) The idealized chemical structures of graphene and P3OT. (b) Schematic of the device with P3OT/graphene thin film as the active layer and the structure ITO/PEDOT:PSS (40 nm)/P3OT:graphene (100 nm)/LiF (1 nm)/Al (70 nm). (c) Energy level diagram of P3OT and SPFGraphene. (d) Schematic representation of the reaction of phenyl isocyanate with GO to form SPFGraphene. (a-c) Reproduced with permission.[22] Copyright 2008, Wiley-VCH.

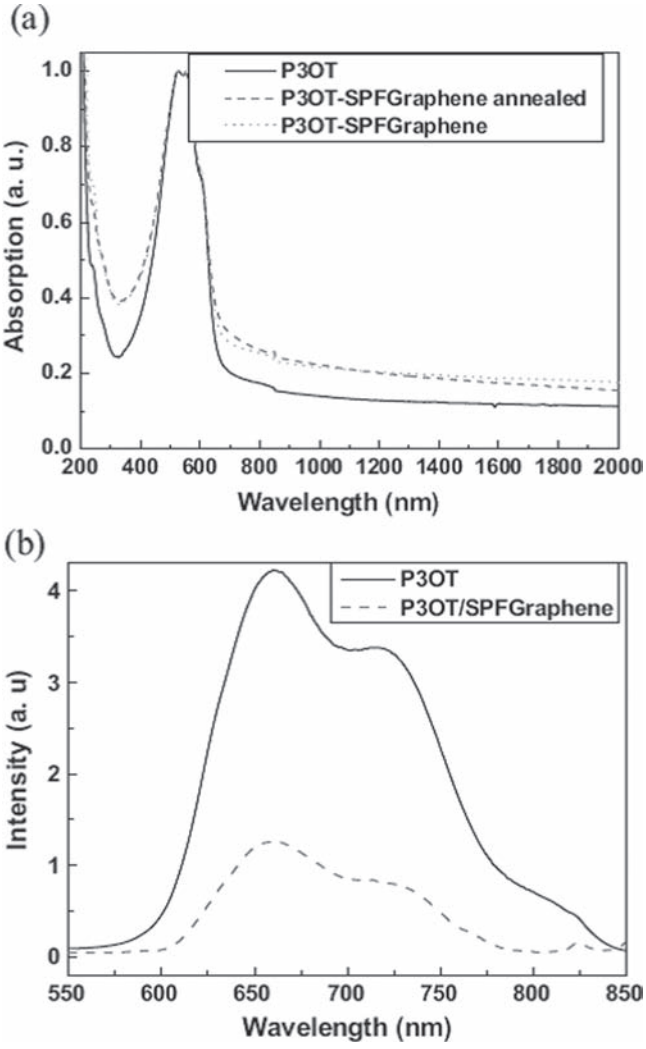

Figure 10. (a) UV-vis-NIR spectra of films of P3OT, P3OT/SPFGraphene, and P3OT/SPFGraphene after annealing. (b) PL spectra of P3OT and P3OT/SPFGraphene composite films at an excitation wavelength of 433 nm. The films were made by spin-coating from solutions of P3OT (15mg mL-1) and P3OT/SPFGraphene (P3OT: 15mg mL-1, SPFGraphene content 5%) at 2000 rpm for 9 s. The films are ca. 100 nm thick. The annealing treatment was conducted at 160 °C for 10 min. (a-b) Reproduced with permission.[22] Copyright 2008, Wiley-VCH.

Chen et al. have reported the fabrication and comprehensive study of the BHJ structure solar cells employing solution processable functionalized graphene (SPFGraphene) as the acceptor and P3OT as the donor (**Figure 9**).[22] Functionalized GO using phenyl isocyanate was carried out to change the hydrophilic nature of the GO sheets to be hydrophobic. As shown in **Figure 10**, the P3OT/SPFGraphene blend film has almost the same absorption as pure P3OT film in the wavelength range 400-650 nm. The strong photoluminescence (PL) of P3OT is remarkably reduced after the introduction of SPFGraphene, showing that efficient energy transfer occurs along the P3OT/SPFGraphene interface. The PL quenching behavior has been in detail studied by Hill et al. through electrochemical studies of GO sheets and P3HT utilizing a surfactant-assisted method.[68] This efficient quenching of PL emission indicates that graphene is a promising electron-accepting material for OPV applications. SPFGraphene based solar cells by spin-coating a dichlorobenzene solution with different ratio of SPFGraphene and P3OT have been studied in details. As shown in **Table 3**, the performance of the P3OT/SPFG-based photovoltaic devices was much higher than that of the devices based on pristine P3OT. Under simulated 100 mW AM 1.5G illumination, a PCE of 0.32% for the P3OT/SPFGraphene-based device with 5% SPFGraphene in the active layer was obtained. After an annealing treatment, the performance of the devices is greatly improved. The device without annealing treatment had a PCE of 0.32%, V_{oc} of 0.56 V, J_{sc} of 2.5 mA/cm^2, and FF of 0.23. After annealing at 160 °C for 20 min, the PCE increased to 1.4%, with V_{oc}, J_{sc}, and FF increasing to 0.92 V, 4.2 mA/cm^2, and 0.37, respectively. At least the following two factors should contribute to the improvement. During the annealing process, graphene sheet should be recovered (partially) again with the removal of the functional groups, resulting in improved charge transport mobility of these graphene sheets. In addition, the morphology of the P3OT matrix can be improved during the annealing process, with an increase in degree of crystallinity and then an enhancement of the charge transport mobility. Similar devices using P3HT/SPFGraphene as the active layer were also fabricated and studied by Chen et al. which show similar OPV performance as that using P3OT, with the highest PCE of 1.10%.[23] Wang and coworkers

Table 3. PV characteristics (V_{oc}, J_{sc}, FF, and PCE) of the devices with the structure ITO/PEDOT:PSS (40 nm)/P3OT:SPFGraphene 100 nm)/LiF (1 nm)/Al (70 nm) under simulated 100 mW AM 1.5G illumination, having different graphene content with different annealing treatment. Reproduced from Ref. [22] with permission from Wiley-VCH.

SPFGraphene content [%]	Annealing		V_{oc} [V]	J_{sc} [mA/cm^2]	FF	PCE%
	Temperature [°C]	Time [min]				
0	No		0.38	0.014	0.18	0.0095
1	No		0.38	0.54	0.26	0.052
1	160	10	0.94	0.37	0.24	0.083
5	No		0.56	2.5	0.23	0.32
5	160	10	0.98	3.2	0.32	0.98
5	160	20	0.92	4.2	0.37	1.4
5	210	10	1.0	3.2	0.31	0.98
15	No		0.38	0.35	0.24	0.034
15	160	10	0.92	0.35	0.25	0.080

also reported similar results using P3HT/SPFGraphene as the active layer with the same device structure.[69–71]

SPFGraphene and functionalized multi-walled carbon nanotubes(f-MWCNTs) are introduced by Liu et al. for BHJ solar cell (**Figure 11**).[72] In the photovoltaic devices based on ITO/PEDOT:PSS/P3HT-f-MWCNTs- SPFGraphene/LiF/Al, P3HT acts as the donor; SPFGraphene acts as the electron acceptor and also provides the percolation paths of electrons; f-MWCNTs provide efficient hole transportation. A PCE of 1.05% was achieved, with V_{oc}, J_{sc} and FF of 0.67 V, 4.7 mA/cm^2 and 0.32, respectively. The authors indicated that SPFGraphene and f-MWCNTs incorporation could enhance carrier mobility and suppress charge recombination, thereby improving photovoltaic action.

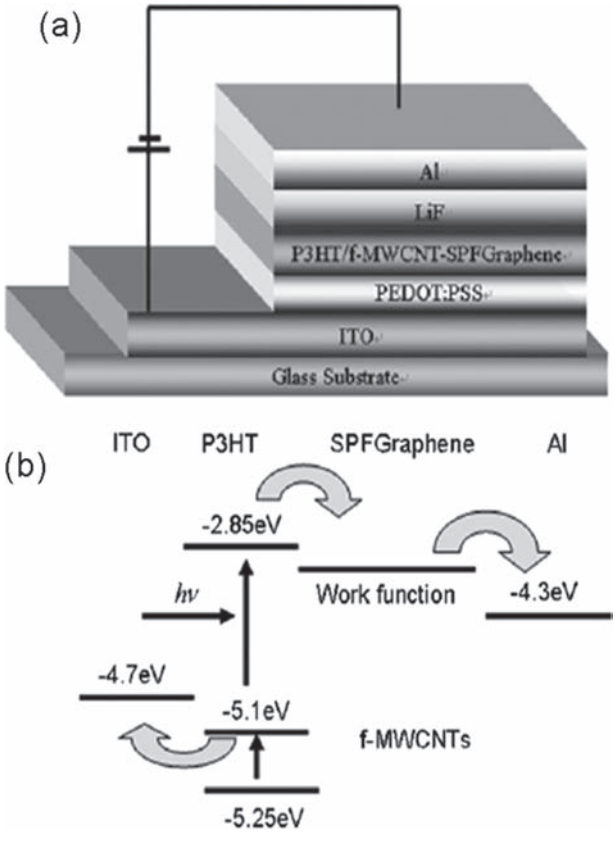

Figure 11. (a) Schematic of the devices with P3HT/f-MWCNT-SPFGraphene as the active layer. (b) Energy band diagram of the fabricated device showing band alignment for SPFGraphene. (a-b) Reproduced with permission.[72] Copyright 2010, Elsevier.

Theoretical and experimental studies have indicated that the band gap and hence optical properties of graphene can be manipulated by reducing its size to the nano level.[73] With high specific surface area for a large interface, high mobility and tunable band gap, graphene quantum dots (GQDs) exhibit great potential as the electron acceptor material in photovoltaic devices. Li et al. reported an electrochemical approach for direct preparation of functional GQDs with a uniform size of 3–5 nm, which exhibited a green luminescence and good stability.[74] Using these GODs as the acceptor, devices with the structure of ITO/PEDOT:PSS/P3HT:GQDs/Al were fabricated. The best performance with a PCE of 1.28%, J_{sc} of 6.33 mA/cm^2, V_{oc} of 0.67 V and FF 0.3 was achieved, which is comparable with most OPV cells using electron acceptors other than fullerenes.[61]

Most recently, Gupta et al. employed aniline functionalized GQDs prepared from graphene sheets (GSs) by a hydrothermal approach as the acceptor to fabricate OPV cells (**Figure 12**).[75] P3HT/ANI-GQDs-based hybrid solar cells were fabricated with the device structure of ITO/PEDOT:PSS/P3HT:ANI-GQDs/LiF/Al. For comparison, the solar cells of P3HT/ANI-GSs were also fabricated. As shown in **Table 4**, the FF of the P3HT/ANI-GQDs heterojunction device is much higher (0.53) than that (0.33) for GSs. The best performance with a PCE of 1.14%, V_{oc} of 0.61V, J_{sc} of 3.51 mA/cm^2, and FF of 0.53 were obtained for 1 wt% ANI-GQD in P3HT. In comparison, maximum values of PCE = 0.65%, V_{oc} = 0.88 V, J_{sc} = 2.65 mA/cm^2, and a low FF = 0.28 were obtained for 10 wt% ANI-GSs in P3HT. In contrast to the large domains (about 100-200 nm diameter) of P3HT/ANI-GSs, AFM images of P3HT/ANI-GQD films show uniform and fine features, suggesting nanoscale phase separation, which

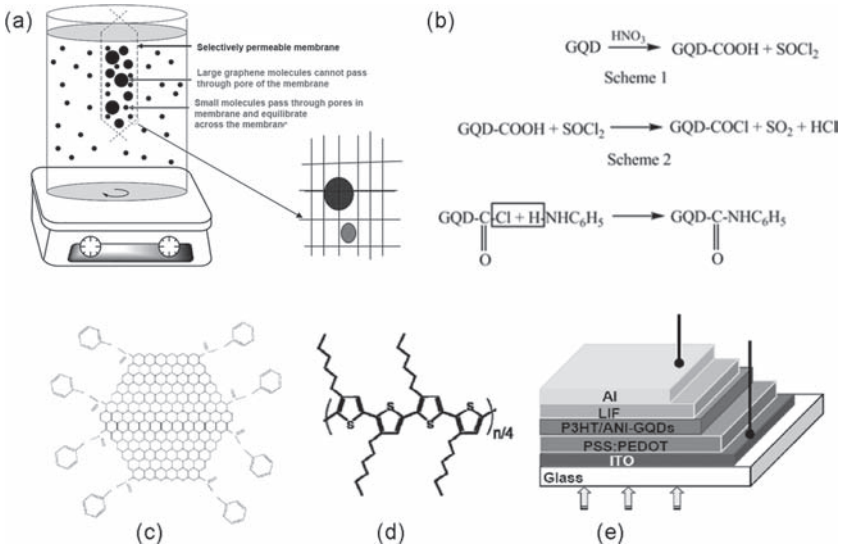

Figure 12. (a) Schematic diagram of the graphene dialysis process; (b) Scheme of functionalization of graphene quantum dot (GQD) with aniline (ANI). (c, d) The idealized chemical structure of ANI-GQD and P3HT. (e) Schematic of the device with P3HT/ANI-GQD thin film as the active layer and the structure ITO/PEDOT:PSS (100 nm)/P3HT:ANI-GQD (100 nm)/LiF (1 nm)/Al (70 nm). Reproduced with permission.[75] Copyright 2011, ACS.

indicates great potentials using GQDs as an acceptor in OPV devices.

C_{60} and its derivatives display remarkable optical and electronic properties. Various hybrid materials based on fullerenes have generated intense attention, driven by the possibility of combining the outstanding properties of the fullerenes with those of other interesting materials. Chen et al. have reported the preparation of graphene-C_{60} hybrid material and studied the nonlinear optical property.[76–78] Recently, Dai and his coworkers reported C_{60}-grafted graphene nanosheets as the electron acceptor in P3HT based BHJ solar cells (**Figure 13**).[79] By a lithiation reaction, mono-substituted C_{60} was covalently attached onto graphene sheets. The devices with C_{60}-Graphene:P3HT exhibited the best performance with a PCE of 1.22%. In contrast, a lower PCE of 0.44% for C_{60}/graphene mixture:P3HT, 0.47% for C_{60}:P3HT were obtained. In addition, these results are much better than those of the devices employing C_{60}-CNT as the acceptors.[80,81] Dai and his coworkers also grafted CH_2OH terminated regioregular P3HT onto carboxylic groups of GO sheets via esterification reaction.[82] A bilayer photovoltaic device based on the solution-cast GO-P3HT with thermally evaporated C_{60} gave a PCE of 0.61%, an ~200% increase compared to that (0.18%) of the device with P3HT/C_{60}.

So far, with the studies of only 2-3 years, the PCEs using graphene as the electron acceptor material have achieved at ~2%, comparable to that about 10 years ago for OPVs using PCBM as the electron acceptor material.[83] Obviously, this is still behind the very recent giant leap for OPV using PCBM.[9] But, considering the intrinsic similarity of C_{60} and graphene materials, and many of the superior properties of graphene, it is believed extremely important to advance the studies in this direction. In this regard, several aspects are worth being considered: 1) the size of graphene. For the BHJ structure devices, the donor-acceptor interface should be maximized for efficient exciton dissociation, and a nanoscale interpenetrating network should be formed for efficient charge transport to the electrodes. Thus, a proper size of graphene comparable to the donor molecular size is important to form a well defined Donor-Acceptor interface and nanoscale interpenetrating network. In general, the size of graphene can be controlled by the oxidation degree and work up process in the preparation GO. In addition, bottom-up synthesis is the most direct approach to obtain certain and uniform size of graphene. 2) The functionalization of graphene and batch-to-batch reproducibility. It is necessary to functionalize for graphene in order to fabricate the device in organic solution process. In general, the performance of OPV cells is very sensitive to even extremely little change of every material and each of the fabrication steps, especially for the active layer. Thus, the batch-to-batch reproducibility of both graphene and the functionalized

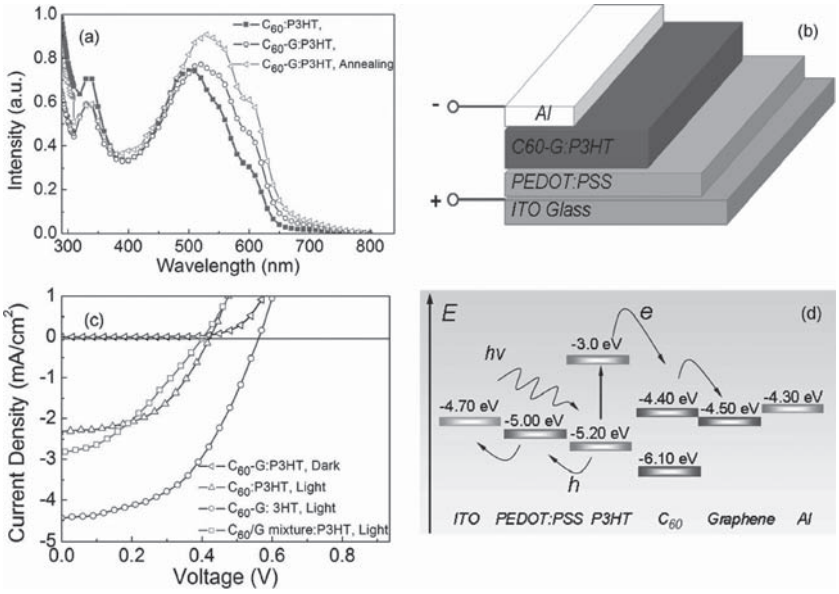

Figure 13. (a) Absorption spectra of the C_{60}-G:P3HT (1:1 wt/wt) film before and after annealing (130 °C, 10min) and the C_{60}:P3HT (1:1 wt/wt) film spin coated onto quartz plates. (b) Schematic of a hybrid photovoltaic device with the C_{60}-G:P3HT composite as the active layer. (c) J-V curve of the photovoltaic devices with the C_{60}-G:P3HT (1:1 wt/wt), the C_{60}:P3HT (1:1 wt/wt), or the C_{60}/G mixture (12 wt% G):P3HT (1:1 wt/wt) as the active layers after annealing treatment (130 °C, 10 min). (d) Energy level diagram for the proposed photovoltaic device using the C_{60}-G:P3HT composite as the active layer. Reproduced with permission.[79] Copyright 2011, ACS.

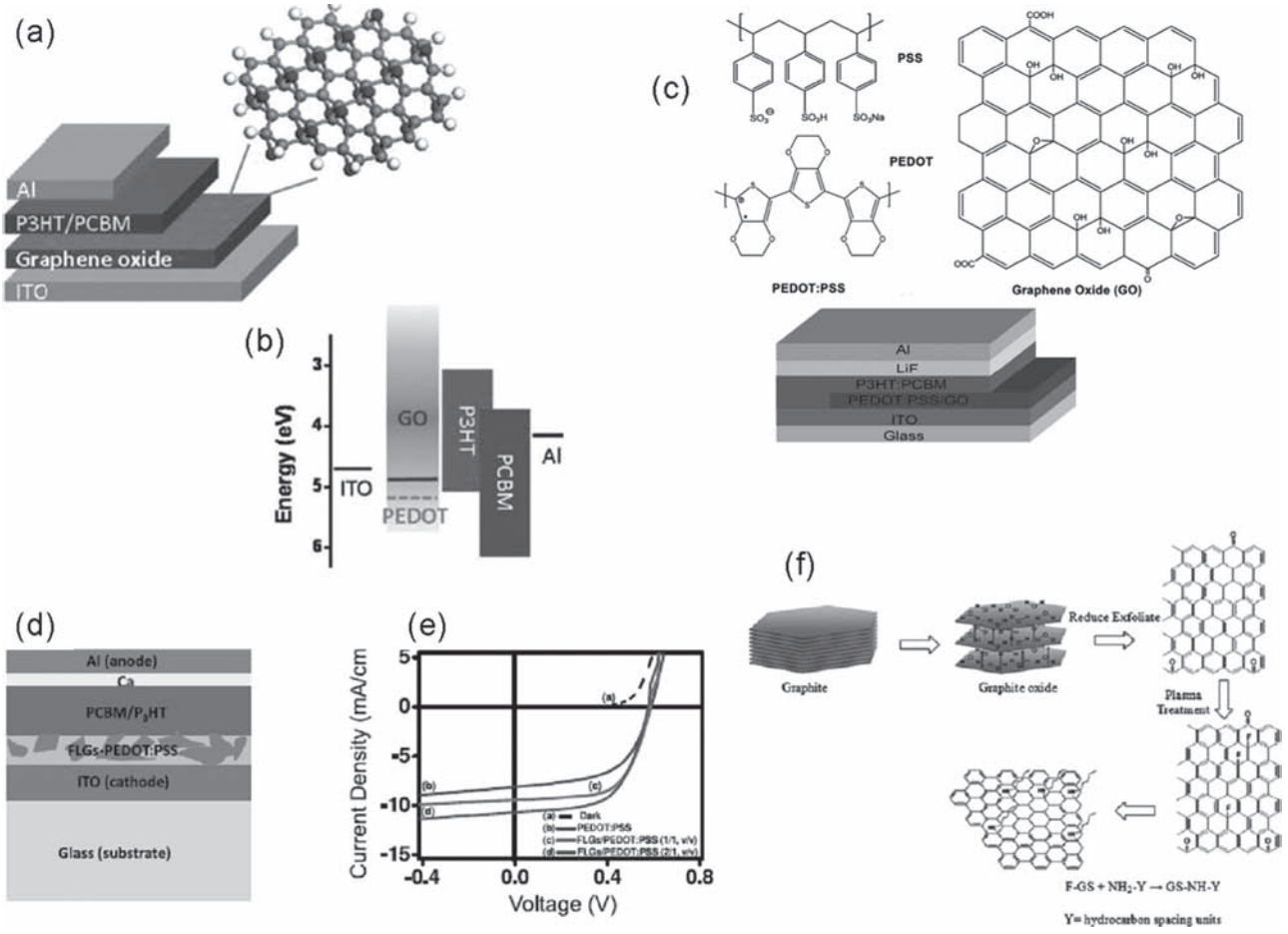

Figure 14. (a) Schematic of the photovoltaic device structure consisting of the following: ITO/GO/P3HT:PCBM/Al. (b) Energy level diagrams of the bottom electrode ITO, interlayer materials (PEDOT:PSS, GO), P3HT (donor), and PCBM (acceptor), and the top electrode Al. (c) The chemical structures of graphene, PEDOT:PSS and schematic structure of photovoltaic device based on PEDOT:PSS/graphene buffer layer. (d) Structure of OPV device with the incorporation of FLG-PEDOT:PSS composite layer and (e) J-V characteristics of photovoltaic devices. (f) Plasma treatment and reaction mechanism with butylamine. (a-b) Reproduced with permission.[87] Copyright 2010, ACS. (c) Reproduced with permission.[88] Copyright 2010, American Scientific Publishers. (d-e) Reproduced with permission.[89] Copyright 2010, IOP Publishing. (f) Reproduced with permission.[90] Copyright 2010, RSC.

graphene need more control. 3) The energy level matching between the donors and graphene. The HOMO and LUMO energy levels of the donor and acceptor need to have optimal offset to maximize the V_{oc}. Furthermore, the energy difference between the LUMOs of the donor and acceptor (graphene), as the driving force for the electron transfer from the donor to the acceptor, should also be considered equally. Partially, this could be achieved by controlling graphene size, layer structure, reduction degree and functionalization. In addition, design and synthesis new donor polymers matching graphene energy level are necessary, because most of the donors nowadays are designed based on the acceptor of fullerene derivatives.

4. Graphene as an Interface Layer Material

The interfaces between active layer and anode and cathode play an essential role in determining the overall device performance of organic electronics.[84] Two excellent reviews have discussed in details the functions and updated progress of the interface layer for OPV cells.[85,86] The main functions of interface materials are: (1) to adjust the energetic barrier height between the active layer and the electrodes; (2) to form a selective and good contact for carriers of one sort; (3) to determine the polarity of the device; (4) to modify the surface property to alter active layer morphology; (5) to prohibit a chemical or physical reaction between the active layer and electrodes; (6) to act as an optical spacer. The discussion about these functions can be found in detail in the above two reviews. Herein, we will discuss the interface layer based on the graphene for OPV.

As the most commonly used HTL in OPVs, acidic PEDOT:PSS is detrimental to the ITO and could introduce water into the device owing to its hygroscopicity, degrading the device performance and life time. Recently, Li et al. have reported that the GO thin film deposited from neutral solutions could act as an effective HTL in OPV cells (**Figure 14**a,b).[87] The average work function of GO thin film samples was measured to be 4.9 eV, higher than the typical value (4.6 eV) obtained for pristine graphene, which matches the work function of ITO and HOMO of P3HT. Incorporating it as an HTL, P3HT:PCBM

Table 4. Performance details of the P3HT/ANI-GQDs and P3HT/ANI-GSs under simulated AM 1.5G 100 mW illumination. Reproduced from Ref. [75] with permission from ACS.

Type of graphene	graphene wt%	V_{oc} (V)	J_{sc} (mA/cm^2)	FF	PCE (%)
–	0	0.43	0.037	0.21	0.003
ANI-GQDs	0.5	0.62	2.65	0.47	0.77
ANI-GSs	0.5	0.71	0.15	0.19	0.02
ANI-GQDs	1	0.61	3.51	0.53	1.14
ANI-GSs	1	0.72	0.19	0.22	0.03
ANI-GQDs	3	0.58	1.32	0.51	0.39
ANI-GSs	3	0.86	0.55	0.27	0.13
ANI-GQDs	5	0.59	0.36	0.52	0.12
ANI-GSs	5	0.94	1.5	0.33	0.46
ANI-GSs	10	0.88	2.65	0.28	0.65
ANI-GSs	15	0.95	0.31	0.25	0.07

BHJ devices were fabricated. ITO-only and conventional device incorporating 30 nm PEDOT:PSS as the HTL were also fabricated for comparison. As shown in **Table 5**, the efficiency values of devices obtained with 2 nm GO as the HTLs was 3.5 ± 0.3%, which was comparable to the devices fabricated with PEDOT:PSS.

Yin et al. and our group reported a composite with GO and PEDOT:PSS as the interface buffer layer between the active layer and the anode (Figure 14c).[88] The device based on pristine PEDOT:PSS buffer layer gives a PCE of 2.1%, J_{sc} of 6.9 mA/cm^2, V_{oc} of 0.60 V, and FF of 0.50. By doping GO in the PEDOT:PSS, the PCE increase to 2.4% with J_{sc} of 10.2 mA/cm^2, V_{oc} of 0.56 V, and FF of 0.42. The J_{sc} value increases by 48%, and the PCE increases by 14%. Obviously, the improvement in the device performance is attributed to the addition of GO. After further optimization, the device showing an PCE value of 3.8%, J_{sc} of 14.2 mA/cm^2, V_{oc} of 0.62 V, and FF of 0.43. The PCE is 1.8 times of that of the pristine PEDOT:PSS buffer layer, and the J_{sc} value reaches 2 times.

Nguyen et al. reported a few-layer graphene nanosheets (FLGs) by ultrasonic treatment of acid-modified expanded graphite in an ammonia-ethanol solution.[89] The FLGs have average thicknesses in the range of 2.6-2.8 nm, corresponding to 8-9 layers. FLG-PEDOT:PSS composite was employed as the HTL (Figure 14d). The device adopting only PEDOT:PSS (Figure 14e) shows J_{sc} of 8.06 mA/cm^2, V_{oc} of 0.58 V, and PCE of 3.10%. For the device using FLGs and PEDOT:PSS at the ratio of 2:1 (v/v), the J_{sc} and PCE increase to 10.68 mA/cm^2 and 3.70%, respectively. The V_{oc} of all the devices are the same (0.58 V), indicating that the energy band alignment within mixed PCBM and P3HT is not influenced by FLG-PEDOT:PSS composite layers.

Table 5. Summary of typical photovoltaic parameters of the control and GO HTL devices. Reproduced with permssion.[87] Copyright 2010, ACS.

	V_{oc} (V)	J_{sc} (mA/cm^2)	FF	PCE (%)
ITO only	0.45	9.84	0.415	1.8 ± 0.2
PEDOT:PSS	0.58	11.15	0.569	3.6 ± 0.2
GO (2nm)	0.57	11.40	0.543	3.5 ± 0.3
GO (4nm)	0.57	10.22	0.339	2.0 ± 0.2
GO (10nm)	0.59	7.84	0.188	0.9 ± 0.2

Valentini et al. reported a method to use soluble chemically derived few-layer graphene sheets (GSs) to modify the HTL.[90] As shown in Figure 14f, chemically functionalized GSs were obtained by covalently attaching fluorine and then exposing the obtained fluorinated graphene sheets to butyl amine (BAM) at room temperature. The devices fabricated with the structure of ITO/PEDOT:PSS/BAM modified F-GSs/RR-P3HT:PCBM/LiF/Al exhibited the best performance with a PCE of 0.74%, compared with that (0.38% and 0.42%) for the devices with non modified GSs and PEDOT:PSS (0.42%), respectively. The results indicate that the butylamine modified GSs can enhance the charge carrier transport and reduce the recombination effect of the active layer.

Obviously, the studies on the interface layer based on graphene just began as for other component materials in OPV devices. Since graphene can be solution processed and its energy level and bandgap can be tuned, it is very likely that graphene can be used as an effective interface layer for OPV cells due to its intrinsic organic/carbon nature. By different functionalization and reduction methods, the energy level of graphene could be tuned. So, in principle, graphene can act not only as the HTL but also as electron transport layer. In practical application for OPV cells it is necessary to understand and control the energy level of graphene or its derivatives to fulfill the requirements of hole transfer or electron transfer. In addition, the wettability of the graphene and its derivatives with their contact layer should be considered when using the solution process.

5. Conclusion

In this Progress Report, the feasibility and versatile applications of graphene materials in OPV cells have been discussed. As for transparent electrodes, graphene has demonstrated

great potential without the detrimental aspects of its traditional analogues. This is based on its high conductivity and transparency, though significant improvement is needed to match the performance of ITO. Solution processing of GO is probably one of its biggest advantages. The band structure of graphene can be tuned through controlling its size, layer, and functionalization. Together with its dispersion ability, these features would make graphene a possible alternative acceptor material for OPV applications, though the performance is still lower than expected. In addition, comparable performances have been achieved employing graphene as the interface layer. One has to keep in mind that these studies are still at the very initial stage, i.e., have been taking place only for 2–3 years. From experience, it is well known that the OPV device performance for a new material can only be determined and judged with intensive and careful optimization. Furthermore, the PCE is more a device parameter than an intrinsic material parameter. Therefore, there is great room and need for the improvement and study of the photovoltaic devices employing graphene for many aspects, whether used as a transparent electrode, active layer or interface layer material. Although the current performance of graphene-based OPV devices is still lower than that with conventional materials, it is believed that employing graphene's excellent electronic properties by tuning its bandgap and energy levels, improving its wetting/soluble ability by versatile functionalization, as well as materializing its superior thermal stability and mechanical integrity, should render graphene a promising material for OPV applications.

Acknowledgements

The authors gratefully acknowledge financial support from the NSFC (Grants 50933003, 50902073 and 50903044), MOST (Grants 2009AA032304, 2011CB932602 and 2011DFB50300) and NSF of Tianjin City (Grant 10ZCGHHZ00600).

Received: July 17, 2011
Revised: August 7, 2011
Published online: September 29, 2011

[1] A. C. Arias, J. D. MacKenzie, I. McCulloch, J. Rivnay, A. Salleo, *Chem. Rev* **2010**, *110*, 3.
[2] C. J. Brabec, V. Dyakonov, U. Scherf, *Organic Photovoltaics: Materials, Device Physics, and Manufacturing Technologies*. John Wiley & Sons, **2008**.
[3] H. Y. Chen, J. H. Hou, S. Q. Zhang, Y. Y. Liang, G. W. Yang, Y. Yang, L. P. Yu, Y. Wu, G. Li, *Nat. Photonics* **2009**, *3*, 649.
[4] S. C. Price, A. C. Stuart, L. Q. Yang, H. X. Zhou, W. You, *J. Am. Chem. Soc.* **2011**, *133*, 4625.
[5] T. Y. Chu, J. P. Lu, S. Beaupre, Y. G. Zhang, J. R. Pouliot, S. Wakim, J. Y. Zhou, M. Leclerc, Z. Li, J. F. Ding, Y. Tao, *J. Am. Chem. Soc.* **2011**, *133*, 4250.
[6] Y. Y. Liang, Z. Xu, J. B. Xia, S. T. Tsai, Y. Wu, G. Li, C. Ray, L.P. Yu, *Adv.Mater.* **2010**, *22*, E135.
[7] H. X. Zhou, L. Q. Yang, A. C. Stuart, S. C. Price, S. B. Liu, W. You, *Angew. Chem. Int. Ed.* **2011**, *50*, 2995.
[8] C. M. Amb, S. Chen, K. R. Graham, J. Subbiah, C. E. Small, F. So, J. R. Reynolds, *J. Am. Chem. Soc.* **2011**, *133*, 10062.
[9] R. F. Service, *Science* **2011**, *332*, 293.
[10] G. Yu, J. Gao, J. C. Hummelen, F. Wudl, A. J. Heeger, *Science* **1995**, *270*, 1789.
[11] A. K. Geim, K. S. Novoselov, *Nat. Mater.* **2007**, *6*, 18.
[12] S. Stankovich, D. A. Dikin, G. H. B. Dommett, K. M. Kohlhaas, E. J. Zimney, E. A. Stach, R. D. Piner, S. T. Nguye, R. S. Ruoff, *Nature* **2006**, *442*, 282.
[13] M. J. Alle, V. C. Tung, R. B. Kaner, *Chem. Rev.* **2010**, *110*, 132.
[14] F. Bonaccorso, Z. Sun, T. Hasan, A. C. Ferrari, *Nat. Photonics* **2010**, *4*, 611.
[15] C. N. R. Rao, A. K. Sood, K. S. Subrahmanyam, A. Govindaraj, *Angew. Chem. Int. Ed.* **2011**, *48*, 7752.
[16] M. I. Katsnelson, *Mater. Today* **2007**, *10*, 20.
[17] H. A. Becerril, J. Mao, Z. Liu, R. M. Stoltenberg, Z. Bao, Y. Chen, *Acs Nano* **2008**, *2*, 463–470.
[18] S. Pang, Y. Hernandez, X. Feng, K. Müllen, *Adv. Mater.* **2011**, *23*, 2779.
[19] J. K. Wassei, R. B. Kaner, *Mater. Today*, **2010**, *13*, 52.
[20] K. S. Novoselov, A. K. Geim, S. V. Morozov, D. Jiang, Y. Zhang, S.V. Dubonos, I.V. Grigorieva, A. A. Firsov, *Science* **2004**, *306*, 666.
[21] Q. Liu, Z. F. Liu, X. Zhang, N. Zhang, L. Y. Yang, S. G. Yin, Y. S. Chen, *Appl.Phys. Lett.* **2008**, *92*, 223303.
[22] Z. F. Liu, Q. Liu, Y. Huang, Y. F. Ma, S. G. Yin, X. Y. Zhang, W. Sun, Y. S. Chen, *Adv. Mater.* **2008**, *20*, 3924.
[23] Q. Liu, Z. F. Liu, X. Y. Zhang, L. Y. Yang, N. Zhang, G. L. Pan, S. G. Yin, Y. Chen, J. Wei, *Adv. Funct. Mater.* **2009**, *19*, 894.
[24] X. Huang, Z. Yin, S. Wu, X. Qi, Q. He, Q. Zhang, Q. Yan, F. Boey, H. Zhang, *Small*, **2011**, *7*, 1876.
[25] M. H. Liang, B. Luo, L. J. Zhi, *Int. J. Energy Res.* **2009**, *33*, 1161.
[26] Y. Q. Sun, Q. Wu, G. Q. Shi, *Energy Enviro. Sci.* **2011**, *4*, 1113.
[27] Y. H. Hu, H. Wang, B. Hu, *ChemSuschem* **2010**, *3*, 782.
[28] X. Wang, L. J. Zhi, K. Mullen, *Nano Lett.* **2008**, *8*, 323.
[29] X. M. Li, H. W. Zhu, K. L. Wang, A. Y. Cao, J. Q. Wei, C. Y. Li, Y. Jia, Z. Li, X. Li, D. H. Wu, *Adv. Mater.* **2010**, *22*, 2743.
[30] M. W. Rowell, M. A.Topinka, M. D. McGehee, H. J. Prall, G. Dennler, N. S. Sariciftci, L. B. Hu, G. Gruner, *Appl. Phys. Lett.* **2006**, *88*, 233506.
[31] D. S. Hecht, L. B. Hu, G. Irvin, *Adv. Mate.* **2011**, *23*, 1482.
[32] I. Forbeaux, J. M. Themlin, J. M. Debever, *Phys. Rev. B* **1998**, *58*, 16396.
[33] K. S. Kim, Y. Zhao, H. Jang, S. Y. Lee, J. M. Kim, K. S. Kim, J. H. Ahn, P. Kim, J.Y. Choi, B. H. Hong, *Nature* **2009**, *457*, 706.
[34] D. A. Dikin, S. Stankovich, E. J. Zimney, R. D. Piner, G. H. B. Dommett, G. Evmenenko, S. T. Nguyen, R. S. Ruoff, *Nature* **2007**, *448*, 457.
[35] G. Eda, M. Chhowalla, *Adv. Mater.* **2010**, *22*, 2392.
[36] S. Park, R. S. Ruoff, *Nat. Nanotechnol.* **2009**, *4*, 217.
[37] Y. F. Xu, G. K. Long, L. Huang, Y. Huang, X. J. Wan, Y. F. Ma, Y. S. Chen, *Carbon* **2010**, *48*, 3308.
[38] J. B. Wu, H. A.Becerril, Z. N. Bao, Z.F. Liu, Y. S. Chen, P. Peumans, *Appl. Phys. Lett.* **2008**, *92*, 263302.
[39] Z. Y. Yin, S. Y. Sun, T. Salim, S. X. Wu, X. Huang, Q. Y. He, Y. M. Lam, H. Zhang, *Acs Nano* **2010**, *4*, 5263.
[40] G. Eda, G. Fanchini, M. Chhowalla, *Nat. Nanotechnol.* **2008**, *3*, 270.
[41] G. Eda, Y. Y. Lin, S. Miller, C. W. Chen, W. F. Su, M. Chhowalla, *Appl. Phys. Lett.* **2008**, *92*, 23305.
[42] J. X. Geng, L. J. Liu, S. B. Yang, S. C. Youn, D. W. Kim, J. S. Lee, J. K. Choi, H. T. Jung, *J. Phys. Chem. C* **2010**, *114*, 14433.
[43] V. C. Tung, L. M. Chen, M. J. Allen, J. K. Wassei, K. Nelson, R. B. Kaner, Y. Yang, *Nano Lett.* **2009**, *9*, 1949.
[44] J. H. Huang, J. H.Fang, C. C. Liu, C.W. Chu, *Acs Nano.* **2011**, DOI: 10.1021/nn201253w
[45] Q. Su, S. P. Pang, V. Alijani, C. Li, X. L. Feng, K. Müllen, *Adv. Mater.* **2009**, *21*, 3191.
[46] X. Wang, L. J. Zhi, N. Tsao, Z. Tomovic, J. L. Li, K. Mullen, *Angew. Chem. Int. Ed.* **2008**, *47*, 2990.

[47] L. G. De Arco, Y. Zhang, A. Kumar, C. W. Zhou, *IEEE T. Nanotechnol.* **2009**, *8*, 135.
[48] Q. K. Yu, J. Lian, S. Siriponglert, H. Li, Y. P. Chen, S. S. Pei, *Appl. Phys. Lett.* **2008**, *93*.
[49] A. Reina, X. T. Jia, J. Ho, D. Nezich, H. B. Son, V. Bulovic, M. S. Dresselhaus, J. Kong, *Large Area, Nano Lett.* **2009**, *9*, 30.
[50] Y. Wang, X. H. Chen, Y. L. Zhong, F. R. Zhu, K. P. Loh, *Appl. Phys. Lett.* **2009**, *95*, 063302.
[51] L.G. Arco, Y. Zhang, C. W. Schlenker, K. Ryu, M. E. Thompson, C. W. Zhou, *Acs Nano* **2010**, *4*, 2865.
[52] M. Choe, B. H. Lee, G. Jo, J. Park, W. Park, S. Lee, W. K. Hong, M. J. Seong, Y. H. Kahng, K. Lee, T Lee, *Org. Electron.* **2010**, *11*, 1864.
[53] G. Jo, S. I. Na, S. H. Oh, S. Lee, T. S. Kim, G. Wang, M. Choe, W. Park, J. Yoon, D. Y. Kim, Y. H. Kahng, T. Lee, *Appl. Phys. Lett.* **2010**, *97*, 213301.
[54] Y. Wang, S. W. Tong, X. F. Xu, B. Özyilmaz, K. P. Loh, *Adv. Mater.* **2011**, *23*, 1514.
[55] H. Park, J. A. Rowehl, K. K. Kim, V. Bulovic, J Kong, *Nanotechnology* **2010**, *21*, 505204.
[56] C. W. Tang, *Appl. Phys. Lett.* **1986**, *48*, 183.
[57] P. Peumans, A. Yakimov, S. R.Forrest, *J. Appl. Phys.* **2003**, *93*, 3693.
[58] D. Markov, J. Hummelen, P. Blom, A. Sieval, *Phys. Rev. B* **2005**, *72*, 45216.
[59] Y. J. Cheng, S. H. Yang, C. S. Hsu, *Chem. Rev.* **2009**, *109*, 5868.
[60] J. W. Chen, Y. Cao, *Acc. Chem. Res.* **2009**, *42*, 1709.
[61] J. E. Anthony, *Chem. Mater.* **2011**, *23*, 583.
[62] Y. X. Liu, M. A. Summers, S. R. Scully, M. D. McGehee, *J. Appl. Phys.* **2006**, *99*, 093521.
[63] Y. J. He, Y. F. Li, *Phys. Chem. Chem. Phys.* **2011**, *13*, 1970.
[64] F. G. Brunetti, X. Gong, M. Tong, A. J. Heeger, F. Wudl, *Angew. Chem. Int. Ed.* **2010**, *49*, 532.
[65] F. G. Brunetti, R. Kumar, F. Wudl, *J. Mater. Chem.* **2010**, *20*, 2934.
[66] J. X. Geng, T. Y. Zeng, *J. Am. Chem. Soc.* **2006**, *128*, 16827.
[67] E. Palacios-Lidon, B. Perez-Garcia, J. Abellan, C. Miguel, A. Urbina, J. Colchero, *Adv. Funct. Mater.* **2006**, *16*, 1975.
[68] C. M. Hill, Y. Zhu, S. Pan, *Acs Nano* **2011**, *5*, 942.
[69] Z. Y. Liu, D. W. He, Y. S. Wang, H. P. Wu, J. G. Wang, *Sol. Energy Mater. Sol. Cells* **2010**, *94*, 1196.
[70] Z. Y. Liu, D. W. He, Y. S. Wang, H. P. Wu, J. G. Wang, *Synth. Met.* **2010**, *160*, 1036.
[71] J. G. Wang, Y. S. Wang, D. W. He, Z. Y. Liu, H. P. Wu, H. T. Wang, Y. Zhao, H. Zhang, B. Y. Yang, *Synth. Met.* **2010**, *160*, 2494.
[72] Z. Y. Liu, D. W. He, Y. S. Wang, H. P. Wu, J. G. Wang, H. T. Wang, *Sol. Energy Mater. Sol. Cells* **2010**, *94*, 2148.
[73] Z. F. Wang, Q. W. Shi, Q. X. Li, X. P. Wang, J. G. Hou, H. X. Zheng., Y. Yao, J. Chen, *Appl. Phys. Lett.* **2007**, *91*, 053109.
[74] Y. Li, Y. Hu, Y. Zhao, G. Q. Shi, L. E. Deng, Y. B. Hou, L. T. Qu, *Adv. Mater.* **2011**, *23*, 776.
[75] V. Gupta, N. Chaudhary, R. Srivastava, G. D. Sharma, R. Bhardwaj, S. Chand, *J. Am. Chem. Soc.* **2011**, *133*, 9960.
[76] X. Y. Zhang, Y. Huang, Y. Wang, Y. F. Ma, Z. F. Liu, Y. S. Chen, *Carbon* **2009**, *47*, 334.
[77] Z. B. Liu, Y. F. Xu, X. Y. Zhang, X. L. Zhang, Y. S. Chen, J. G. Tian, *J. Phys. Chem. B* **2009**, *113*, 9681.
[78] X. Y. Zhang, Z. F. Liu, Y. Huang, X. J. Wan, J. G. Tian, Y. F. Ma, Y. S. Chen, *J. Nanosci. Nanotechnol.* **2009**, *9*, 5752.
[79] D. S. Yu, K. Park, M. Durstock, L. M. Dai, *J. Phys. Chem. Lett.* **2011**, *2*, 1113.
[80] C. Li, Y. L. Chen, S. A. Ntim, S. Mitra, *Appl. Phys. Lett.* **2010**, *96*, 143303.
[81] C. Li, S. Mitra, *Appl. Phys. Lett.* **2007**, *91*, 253112.
[82] D.S. Yu, Y. Yang, M. Durstock, J. B. Baek, L. M. Dai, *Acs Nano* **2010**, *4*, 5633.
[83] C. J. Brabec, S. N. Sariciftci, *Monatsh. Chem.* **2001**, *132*, 421.
[84] H. Ma, H. L. Yip, F. Huang, A. K. Y. Jen, *Adv. Funct. Mater.* **2010**, *20*, 1371.
[85] R. Steim, F. R. Kogler, C. J. Brabec, *J. Mater. Chem.* **2010**, *20*, 2499.
[86] L. M. Chen, Z. Xu, Z. R. Hong, Y. Yang, *J. Mater. Chem.* **2010**, *20*, 2575.
[87] S. S. Li, K. H. Tu, C. C. Lin, C. W. Chen, M. Chhowalla, *Acs Nano* **2010**, *4*, 3169.
[88] B. Yin, Q. Liu, L.Y. Yang, X. M. Wu, Z. F. Liu, Y. L. Hua, S. G. Yin, Y. S. Chen, *J. Nanosci. Nanotechnol.* **2010**, *10*, 1934.
[89] D. D. Nguyen, N. H. Tai, Y. L. Chueh, S. Y. Chen, Y. J. Chen, W. S. Kuo, T. W. Chou, C. S. Hsu, L. J. Chen, *Nanotechnology* **2011**, *22*, 295606.
[90] L. Valentini, M. Cardinali, S. B. Bon, D. Bagnis, R. Verdejo, M. A. Lopez-Manchado, J. M. Kenny, *J. Mater. Chem.* **2010**, *20*, 995.